ADVANCED MATERIALS TECHNOLOGIES
www.advmattechnol.de

# Catalyzing Viologen Electrochromic Reaction with $CuO_x$ Nanoparticles

*Liangliang Wu, Huajing Fang,* Jiaqi Li, Lingqi Wu, and Hong Wang**

**Viologen-based electrochromic devices have attracted great attention because of their tremendous potential in building energy conservation and low power display. However, the unsatisfactory performance at lower voltage limits their application, while the high driving voltage increases the energy consumption as well as safety risk. Herein, an electrocatalytic strategy is proposed for high-performance viologen-based electrochromic devices. Copper oxide ($CuO_x$) nanoparticles are uniformly deposited on the F-doped Tin Oxide (FTO) glass for enhancing the catalytic activity of $Br^-/Br_3^-$ redox couple, thereby promoting the interfacial charge transfer. The driving voltage can be reduced by ≈30% without sacrificing its high transparency (up to 80%) and the cycling stability can be significantly improved within 200 cycles. Large-area smart windows and electrochromic displays are fabricated, which can be driven by the 1.5 V dry battery. This work opens up a new path to optimize the electrochromic performance of viologens and also lays the foundation for the application of catalysis in optoelectronic devices.**

## 1. Introduction

Energy saving and green low-carbon technology have become critical to the sustainable development of human society in recent years.[1–3] Electrochromic device, referring to the reversible change of optical properties upon the application of a suitable voltage, is a promising energy-saving gadget for regulating heat flux in architectures.[4–8] Among all the electrochromic materials, viologen (1,1′-substituted-4,4′-bypyridinium salt) has received widespread attention due to its unique advantages over inorganic compounds, such as rich color assortment, high coloration efficiency, large transmittance contrast and simple device construction.[9–12] Their electrochromic mechanism is based on the redox reaction between the three states including the di-cation ($V^{2+}$, bleached), radical cation ($V^+$, colored), and di-reduced neutral compound ($V^0$, colored).[13–15] Since the di-cation state is the most stable of the three, the colored viologen radical cation and di-reduced neutral species tend to recombine with oxidized anion under open circuit (known as self-bleaching). Therefore, a continuous external voltage is required to maintain the colored state. Moreover, the spontaneous self-bleaching reaction leads to a high driving voltage to initiate the coloring process. The high driving voltage not only increases the energy consumption during the spectral modulation, but also challenges the electrochemical window of devices, which seriously restricts the application of viologen electrochromic materials. In order to address this long-standing issue, various approaches have been investigated to enhance the electrochromic performance of the devices at lower voltage. For example, Hsiao et al. realized a low driving voltage electrochromic device based on *N*-methylphenothiazione ionic liquid through selecting the two electrode materials with close electrochemical potentials.[16] Zhang et al. modified the electrochromic molecules of phthalate derivatives with polyaromatic esters to enlarge the conjugated area and lower the reduction potentials of the small molecule organic electrochromic materials.[17] Kobayashi et al. introduced ferrocene in the electrolyte solution as counter redox material to improve the cycling durability and reduce the driving voltage.[18] These preliminary works provide feasible strategies starting from electrolytes and electrochromic chromophores. However, there are still some inescapable obstacles such as the complex synthesis process and the interference from the colored additives. It is urgent to seek a more general and convenient strategy for low-driving voltage and high-performance electrochromic devices.

Viologen-based electrochromic devices are normally multilayer electrochemical cells, containing two electrodes and an electrolyte with dissolved viologen cations and redox anions.[19–21] During the coloring process, viologen cations undergo a reduction reaction on the working electrode, while the anions undergo an oxidation reaction on the counter electrode to achieve charge balance. Thus, the driving voltage is theoretically

---

L. Wu, H. Fang, J. Li, L. Wu
State Key Laboratory for Mechanical Behavior of Materials
School of Material Science and Engineering
Xi'an Jiaotong University
Xi'an 710049, China
E-mail: fanghj@xjtu.edu.cn

L. Wu
School of Semiconductor and Physics
North University of China
Taiyuan 030051, China

H. Wang
Department of Materials Science and Engineering
Southern University of Science and Technology
Shenzhen 518055, China
E-mail: wangh6@sustech.edu.cn

The ORCID identification number(s) for the author(s) of this article can be found under https://doi.org/10.1002/admt.202301028

**DOI: 10.1002/admt.202301028**

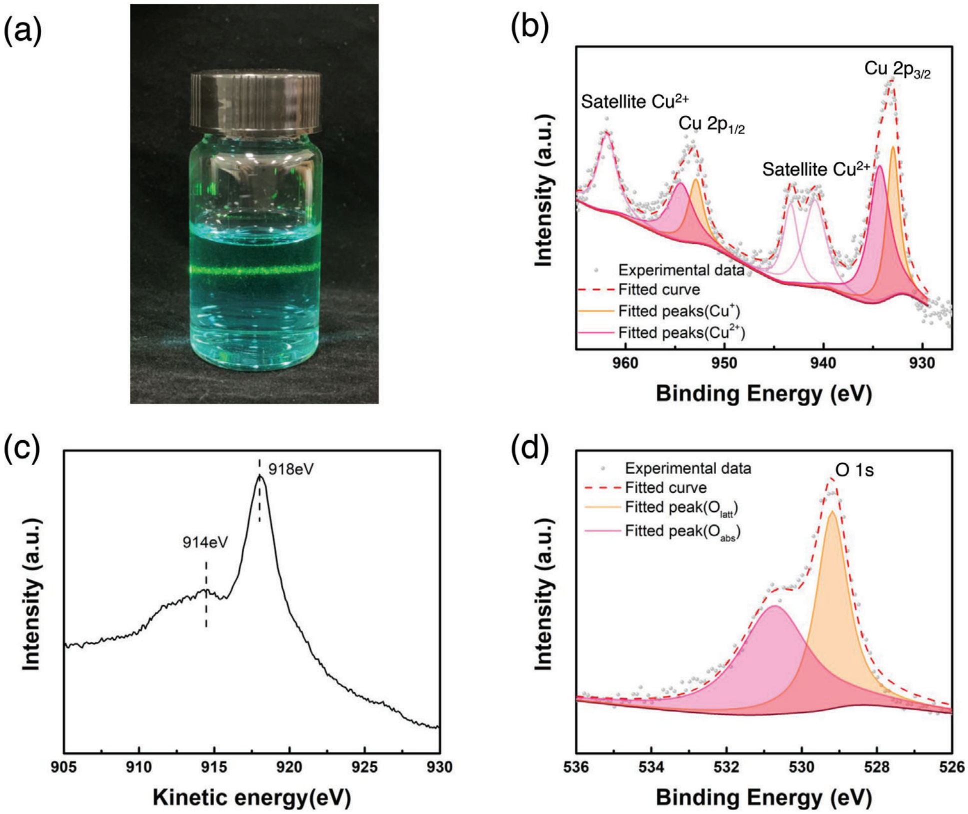

**Figure 1.** a) Photograph of the $CuO_x$ colloidal precursor, Tyndall effect was visible when irradiated with a green laser beam. b) XPS spectra of Cu 2p in the copper oxide. c) Auger spectra of Cu LMM. d) XPS spectra of O 1s in the copper oxide.

determined by the difference between the oxidation potential of oxidizable species on the working electrode and the reduction potential of reducible species on the counter electrode.[22,23] In this regard, the counter electrode also affects the electrochromic behaviors. Inspired by dye-sensitized solar cells and other photoelectric conversion devices, it is a promising approach to optimize the performance of electrochromic devices by boosting the catalytic property of counter electrodes.[24–26] In fact, electrocatalysis is an effective means to promote electrochemical reactions and has been widely used in various energy and environment applications.[27–30] To the best of our knowledge, viologen-based electrochromic devices with an electrocatalytic counter electrode have not been reported so far.

Nowadays, copper oxide ($CuO_x$) nanomaterials have attracted extensive attention because of the readily available catalytic activity, low cost, and environmentally friendly advantages, compared with Au, Pt, Pd, and other precious metals.[31–33] Moreover, copper oxide nanomaterials can be fabricated by a facile solution process, with a flexible morphology control ability.[34,35] In this work, we demonstrated a $CuO_x$ modified FTO glass ($CuO_x$/FTO) as the electrocatalytic counter electrode in viologen-based electrochromic devices. Notably, the $CuO_x$ is distributed as nanoparticles on the surface of FTO electrode, which can provide catalytic sites without sacrificing the transparency of the total electrochromic device. The driving voltage was significantly reduced and the cycling stability was obviously enhanced in the electrochromic devices with $CuO_x$/FTO counter electrode, compared that with a bare FTO counter electrode. The electrochemical behavior of the electrochromic device with $CuO_x$/FTO counter electrode was systematically exploited by cyclic voltammetry and DFT calculation. In addition, large-area electrochromic devices were fabricated by spraying technology to demonstrate the practicality of these $CuO_x$/FTO electrocatalytic counter electrodes.

## 2. Results and Discussion

Copper oxide is selected as the electrocatalytic material for the counter electrode of the electrochromic device, which is prepared by a simple sol-gel method. **Figure 1**a shows the photograph of copper oxide precursor, in which the significant Tyndall phenomenon indicates the colloidal property of the precursor. Then, the copper oxide was fabricated by spin coating the precursor on FTO substrates. The chemical valences of Cu and O in the copper oxide were investigated by X-ray photoelectron spectroscopy. The survey scan in Figure S1 (Supporting Information) shows the Cu 2p photoelectron peaks, O 1s peaks and the photoelectron peak of the adventitious carbon (C 1s). The high-resolution Cu 2p spectra in Figure 1b consists of two groups of peaks, corresponding to Cu $2p_{3/2}$ and Cu $2p_{1/2}$. The main peaks of Cu $2p_{3/2}$ (933.9 eV) and Cu $2p_{1/2}$ (953.8 eV) with a gap of 19.9 eV coincident with the standard CuO spectrum.[36] In addition to the main peaks, the appearance of satellite peaks also indicates the presence of $Cu^{2+}$, which is due to unfilled 3d shell

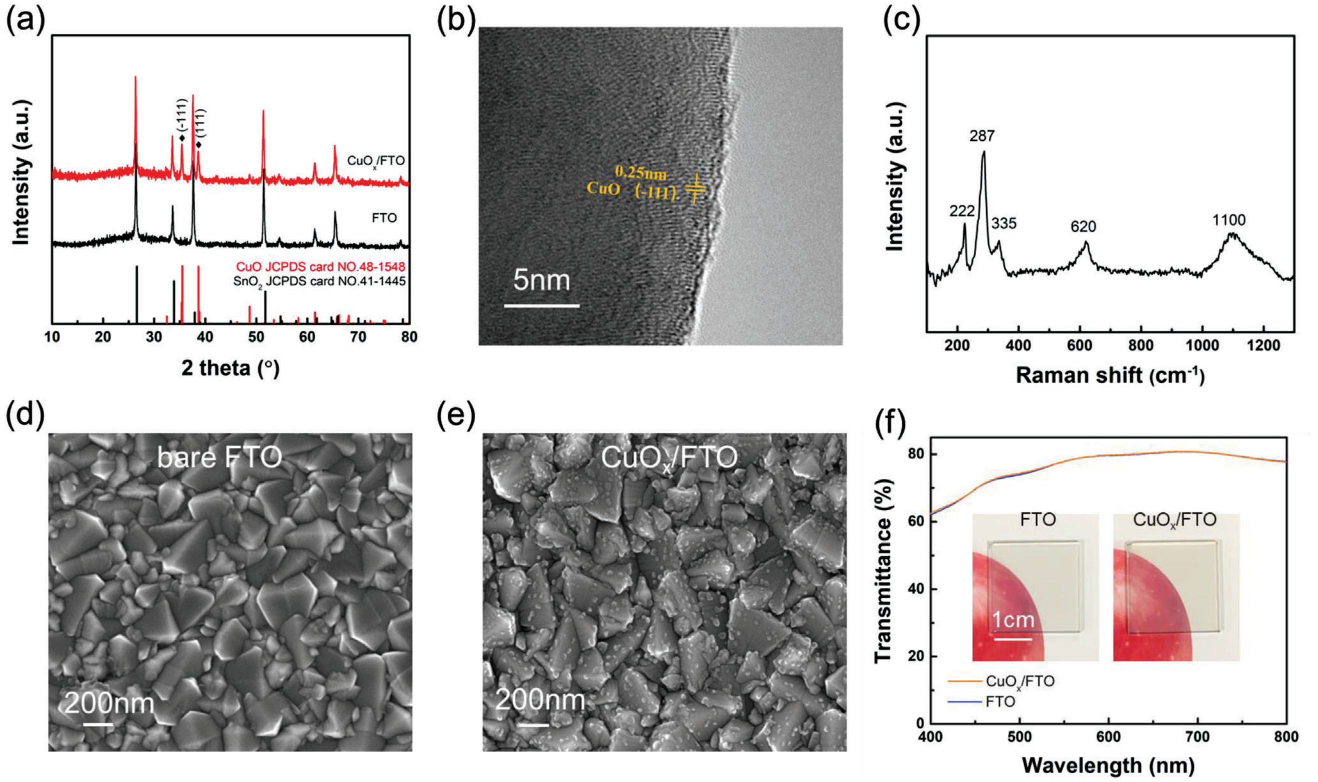

**Figure 2.** a) XRD patterns of the CuO$_x$/FTO and FTO electrodes. b) HRTEM image of prepared CuO$_x$ nanoparticles. c) Raman spectrum of the CuO$_x$/FTO electrode. d) SEM of the FTO electrode. e) SEM of the CuO$_x$/FTO electrode. f) Transmittance of the CuO$_x$/FTO and FTO electrodes in the wavelength range from 400 to 800 nm.

of $Cu^{2+}$.[37] When the intensity ratio of the satellite peak to main peak is 0.55–0.57, there is only $Cu^{2+}$.[38] However, the intensity ratio is calculated to be 0.47 in Figure 1b, which means the coexistence of $Cu^{2+}$ and reduced copper species ($Cu^+$ or $Cu^0$) synchronously. To further confirm the valence state of copper element, Auger spectra of the sample has been measured. As shown in Figure 1c, the peaks located at 914 and 918 eV in Auger spectra of Cu LMM were assigned to $Cu^+$ and $Cu^{2+}$ respectively.[39] Therefore, reduced copper species can be identified as $Cu^+$, and the main peaks of Cu $2p_{3/2}$ and Cu $2p_{1/2}$ can be fitted by $Cu^{2+}$ and $Cu^+$ in Figure 1b. The peaks at binding energies of 934.2 and 954.4 eV are ascribed to $Cu^{2+}$, and the peaks at binding energies of 932.9 and 952.8 eV are ascribed to $Cu^+$. The $Cu^+$ fraction derived from Cu $2p_{3/2}$ peak is ≈40%, which means that the $CuO_x$ contains both $Cu^+$ and $Cu^{2+}$ and the $Cu^{2+}$ is dominant. Besides, the O 1s spectra in Figure 1d is fitted by two peaks at binding energies of 529.1 and 530.7 eV. The strong peak at 529.1 eV is characteristic of lattice oxygen ($O_{latt}$) in the $CuO_x$. While the peak at 530.7 eV is attributed to the adsorbed oxygen ($O_{abs}$) in $OH^-$ and $CO_3^{2-}$, which is adsorbed by active sites on the sample surface.[40]

The crystallographic phase of the as-prepared $CuO_x$ was investigated via X-ray diffraction pattern, high resolution transmission electron microscopy (HRTEM) and Raman spectrum. In **Figure 2**a, the characteristic peaks at 35.5° and 38.8° correspond to the (−111) and (111) diffraction planes of monoclinic CuO (JCPDS card No. 48–1548).[41,42] HRTEM image of $CuO_x$ nanoparticles in Figure 2b demonstrated interplanar spacing of 0.25 nm that corresponds to (−111) planes of monoclinic CuO.[43,44] Besides, the interplanar distance of (−111) can be calculated by the Bragg's Law:

$$D_{(-111)} = \frac{\lambda}{2\sin\theta_{(-111)}} \tag{1}$$

where $\lambda$ is wavelength of the X-ray used ($\lambda = 0.154$ nm) and $\theta$ is the Bragg angle of the (−111) diffraction peak ($2\theta = 35.5°$). Consequently, the calculated interplanar distance of (−111) is 0.265 nm, which is basically consistent with the HRTEM result. Moreover, elemental mapping analysis by energy dispersive X-ray spectrometer of the $CuO_x$ nanoparticles in Figure S2 (Supporting Information) reveals the exist of Cu and O elements, which also confirms the chemical composition of $CuO_x$. The Raman spectrum was carried out to further analyze the crystal structure of $CuO_x$ in Figure 2c. The Raman peak at 222 cm$^{-1}$ is associated with $2E_u$ vibration mode of Cu—O—Cu bond in $Cu_2O$, while three Raman peaks at 287, 335, and 620 cm$^{-1}$ correspond to the $A_g$, $B_g{}^1$ and $B_g{}^2$ vibration modes of Cu—O bond in CuO.[45] Moreover, the Raman peak observed at 1100 cm$^{-1}$ is related to multiphonon scattering processes in CuO.[46] Since Raman spectroscopy shows the presence of $Cu_2O$, but this compound was not detected by XRD, it is likely that the amount of $Cu_2O$ formed is small and $Cu_2O$ phase is on the surface of the nanoparticles therefore cannot be detected by XRD.[47] Thus, it can be inferred that the $CuO_x$ sample contains both CuO and $Cu_2O$, which is consistent with the previous analysis in Figure 1.

The morphology of bare FTO and $CuO_x$ modified FTO glass was observed by field emission scanning electron microscopy. As shown in Figure 2d,e, the FTO electrode itself is a polycrystalline film containing micron-sized $SnO_2$ grains and the $CuO_x$ nanoparticles are evenly distributed on $SnO_2$ grains to form a hierarchical structure. Besides, the elemental analysis by energy dispersive X-ray spectrometer reveals that Cu element is present on the FTO electrode (Figure S3, Supporting Information). Thus, the $CuO_x$ nanoparticles were deposited on FTO electrode successfully, which can provide catalytic sites for electrochemical reactions. Through the statistically analyzing the particle sizes in Figure 2e (as shown in Figure S4, Supporting Information), the $CuO_x$ nanoparticles are much smaller in size (≈35.67 nm) than the wavelength of visible light. This CuOx/FTO hierarchical structure is believed to maintain the high transmittance of the FTO electrode and provide more catalytic sites for the redox reactions. The transmittance spectrum of the $CuO_x$/FTO electrode is shown in Figure 2f, compared with that of bare FTO electrode. The two electrodes possess up to 80% transmittance in the wavelength range from 400 to 800 nm. This is mainly due to the spectral absorption of FTO, and the introduction of $CuO_x$ nanoparticles does not affect the transmittance as expected. In addition, the inset in Figure 2f also proved the similar high transparency for both electrodes, which satisfies the requirement of counter electrode in electrochromic devices.

The schematic diagram of the electrochromic device is shown in **Figure 3**a, in which $CuO_x$/FTO and bare FTO glasses served as the counter electrode and working electrode, respectively. The ethyl viologen dibromide electrolyte is filled between the two electrodes to form a complete sandwich electrochromic device. In this work, the electrochromic device with same construction but bare FTO counter electrode was used as the control sample. The devices with different counter electrodes have similar transmittance at 0 V as shown in Figure 3b. When applying a voltage of 1.3 V, the transmittance of the device with $CuO_x$/FTO counter electrode decreases significantly, while the transmittance of the control sample with FTO counter electrode is almost unchanged. It indicates that the device with bare FTO counter electrode has a driving voltage higher than 1.3 V, and the introduction of $CuO_x$ nanoparticles on counter electrode can reduce the driving voltage of the electrochromic device.

Then the transmittance-time curve was tested to investigate the dynamic characteristics of electrochromic devices. By applying 1.8 V voltage for 90 s and 0 V voltage for 120 s periodically, the transmittance at 600 nm changes accordingly as shown in Figure S5 (Supporting Information). Under the same conditions, electrochromic device with $CuO_x$/FTO counter electrode and FTO counter electrode possesses similar transmittance modulation performance. This may be due to that the electrochemical reactions in both devices can be completely carried out under sufficient reaction time. In the early stage of the coloring process, the switching speed the electrochromic device with CuOx/FTO counter electrode are better than that of the control sample, which indicates that the introduction of CuOx is beneficial for enhancing the electrochemical reaction rate. Moreover, the coloration efficiency (CE) of these devices, which is an important parameter to measure electrochromic performance, can be calculated as follows,[48,49]

$$\mathrm{CE} = \frac{\Delta OD}{\Delta Q} = \frac{\log\left(T_b/T_c\right)}{\Delta Q} \tag{2}$$

where ΔOD is the change in optical density, $T_b$ and $T_c$ are the corresponding transmittances of the device in the bleached and colored states and ΔQ is the inserted charge, which can be obtained by current integration in chronoamperometry curve. In Figure 3c,d, the plots of the optical density versus injected charge density during the coloring process are obtained from the transmittance-time characteristic and chronoamperometry curve in Figures S6 and S7 (Supporting Information). The CE can be calculated from the slope of the △OD versus the injected charge density, which should be 127.06 and 108.58 $cm^2\ C^{-1}$ corresponding to the electrochromic device with $CuO_x$/FTO counter electrode and FTO counter electrode respectively. They are coincident with the viologen-based electrochromic device. And the similar coloration efficiency between the two devices indicates that the $CuO_x$ nanoparticles only catalytic electrochemical reaction and do not participate in electrochemical reactions.

Besides, the cycling stability of the coloration process was also measured to evaluate the practicality of the electrochromic device. Figure 3e,f shows the transmittance-time characteristic of the electrochromic device with CuOx/FTO and FTO counter electrode under pulse voltage of 1.8 V for 10 s and 0 V for 60 s for 380 cycles respectively. The transmittance modulation remains ≈47.35% over 380 cycles in the electrochromic devices with CuOx/FTO counter electrode, compared with gradually decreased transmittance modulation in the electrochromic devices with a bare FTO counter electrode. In addition, the cycling stability performance of both devices decreased during the cycles, which may be related to the oxidation of bromine ions. Therefore, optimizing electrolyte composition and exploring the decaying mechanism can be one of the investigation aspects in the further.

To evaluate the electrochemical behavior during the coloring process, the cyclic voltammograms of the devices with $CuO_x$/FTO counter electrode and FTO counter electrode in two-electrode system were tested. As shown in **Figure 4**a, there are two reduction peaks in the process of applying negative voltage, which corresponds to the two-step redox reaction of viologen.[50,51] Among them, the first reduction peak corresponds to the process in which the di-cations obtain electrons and be reduced to monovalent viologen cations. While the oxidation peak at ≈0 V corresponds the process in which the monovalent viologen cations can be oxidized to di-cations state.[52–54] And the electrochromic phenomenon of viologen-based electrochromic devices usually appears at the first reduction peak of viologen due to the large difference of the molar absorption between the di-cations and monovalent viologen cations. Thus, it is obvious that the electrochromic device with $CuO_x$/FTO counter electrode demonstrates a lower driving voltage (1.3 V) compared to the control sample with FTO counter electrode. To further analyze the catalytic effect of the counter electrode, the cyclic voltammogram of the $CuO_x$/FTO electrode and FTO electrode were tested by the electrochemical workstation in three-electrode system. The redox

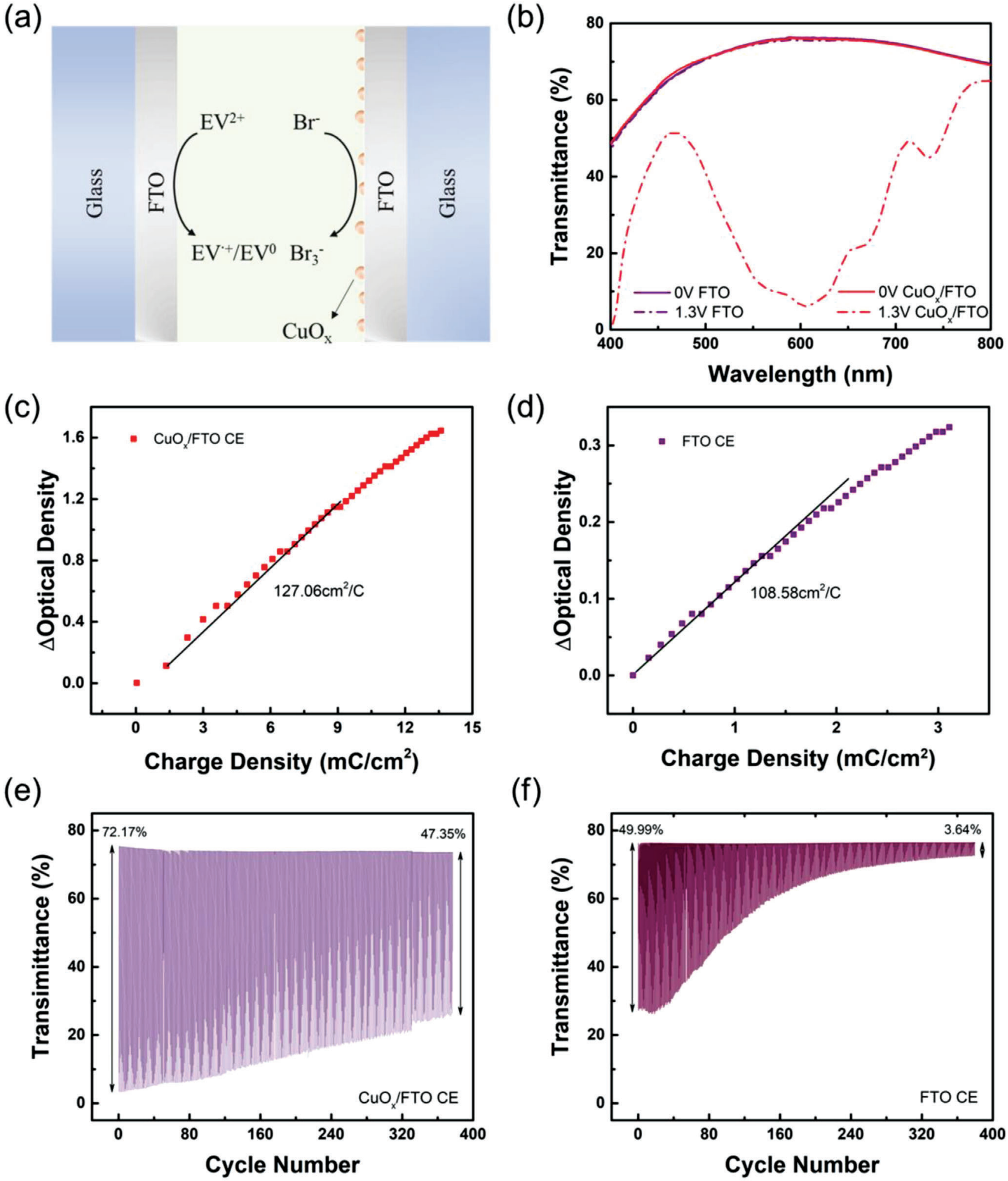

**Figure 3.** a) The schematic diagram of the electrochromic device with $CuO_x$/FTO counter electrode. b) Transmittance of the electrochromic device with $CuO_x$/FTO and FTO counter electrode in 0 and 1.3 V respectively. c) Plots of the optical density versus injected charge density during the coloring process of the electrochromic device with $CuO_x$/FTO and FTO counter electrode. d) Plots of the optical density versus injected charge density during the coloring process of the electrochromic device with FTO counter electrode. e) Cycling stability performance of the electrochromic device with $CuO_x$/FTO counter electrode under pulse voltage of 1.8 V for 10 s and 0 V for 60 s. f) Cycling stability performance of the electrochromic device with FTO counter electrode under pulse voltage of 1.8 V for 10 s and 0 V for 60 s.

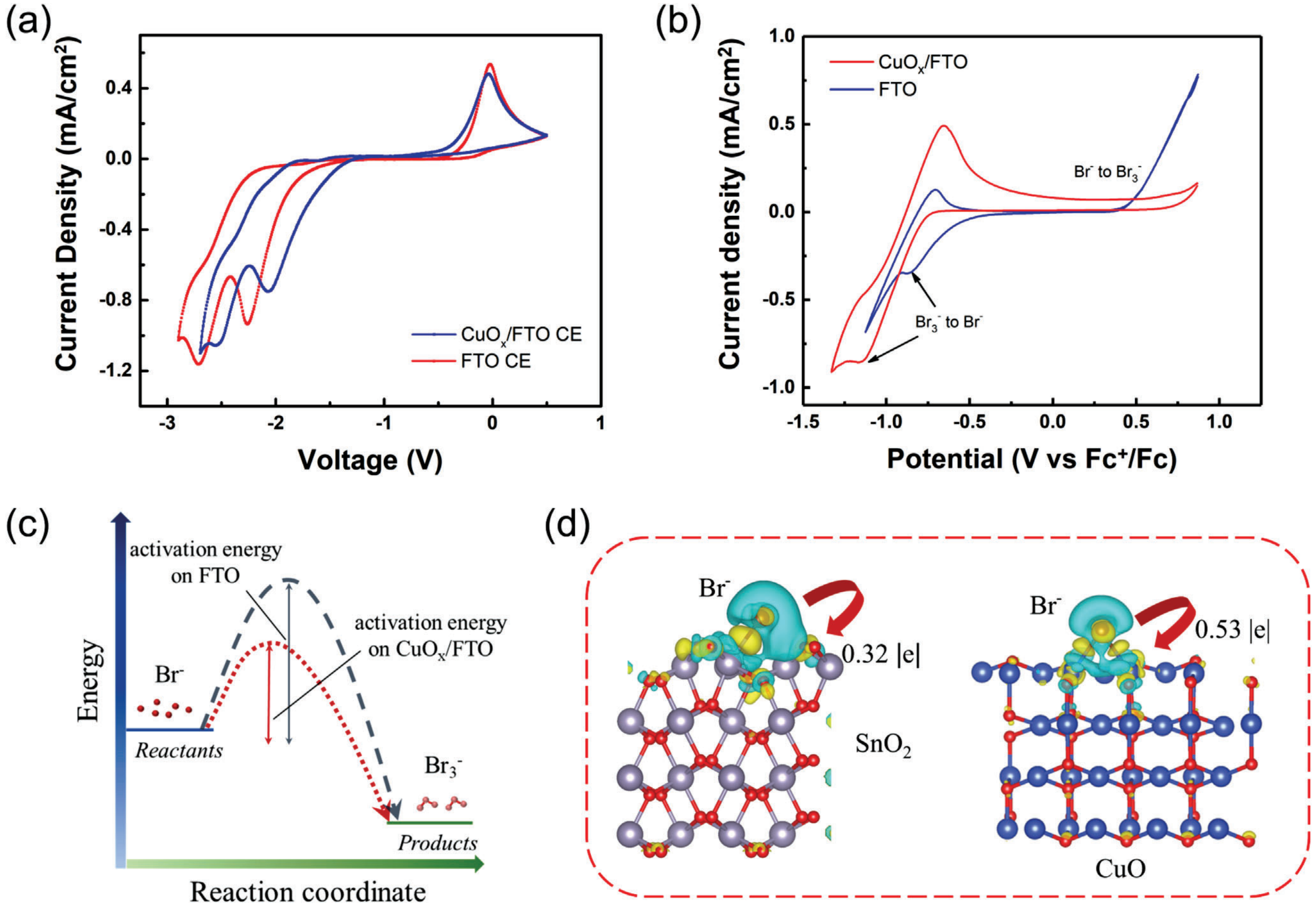

**Figure 4.** a) The cyclic voltammogram of the device in two-electrode system with a scan speed of 50 mV s$^{-1}$. b) The cyclic voltammogram of the CuO$_x$/FTO and FTO electrodes in three-electrode system with a scan speed of 10 mV s$^{-1}$. c) The energetic schematic diagram of the oxidation reaction from Br$^-$ to Br$_3$$^-$ on CuO$_x$/FTO electrode. d) The diagrams of the calculated charge density difference on the surface of CuO and SnO$_2$ model. The dark blue, red, gray, and gold balls represent the Cu, O, Sn, and Br atoms, respectively.

reaction on the CuO$_x$/FTO and FTO counter electrodes is shown as follows,

$$3Br^{-}\,(aq) \leftrightarrow Br_3^{-}\,(aq) + 2e^{-} \tag{3}$$

Figure 4b shows that the redox current on the CuO$_x$/FTO electrode surface starts to increase at lower voltage, which means the oxidation reaction potential of Br$^-$ was reduced on the CuO$_x$/FTO electrode surface compared to that on the bare FTO electrode surface. At the same time, Nyquist plots of the electrochemical impedance spectroscopy are shown in Figure S8 (Supporting information). The CuO$_x$/FTO electrode possesses smaller semicircle diameter in the low-frequency region compared to that of the FTO electrode, which indicates the smaller charge transfer resistance at the interface between the CuO$_x$/FTO electrode and electrolyte.[55] These results are consistent with reduced driving voltage of the electrochromic device with CuO$_x$/FTO counter electrode. The mechanism can be revealed by the energetic schematic diagram in Figure 4c. In general, reactants require enough kinetic energy to overcome the energy barrier to form products.[56] The CuO$_x$ nanoparticles on the FTO electrode surface can absorb Br$^-$ ions and work as the catalyst, which reduces the energy barrier (activation energy) for the oxidation reaction from Br$^-$ to Br$_3$$^-$. Thus, the driving voltage of the electrochromic device is reduced. In order to obtain the deep understanding into the high catalytic activity of the counter electrode, we performed the density functional calculation (DFT). As a comparison, the charge density difference for the copper oxide and tin oxide (SnO$_2$, stands for bare FTO counter electrode) systems was calculated respectively, which can be used to analyze the catalytic properties theoretically.[57,58] Figure 4d shows the calculated results of charge density difference of the two different systems. The electrons tend to be transferred to counter electrodes when the Br$^-$ ions are adsorbed on the electrode surface, which was beneficial for further oxidation. Compared to the bare FTO counter electrode system, there is a stronger electron interaction between the adsorbed Br$^-$ ion and copper oxide surface, thereby lowing the oxidation reaction potential of Br$^-$ ion. The DFT results are consistent with the experimental results, proving that the CuO$_x$ catalyst can improve the electrochromic performance of the entire device by boosting the reactions at the interface between electrolyte and counter electrode.

Next, we developed two kinds of large area electrochromic devices to verify the practicality of the CuO$_x$/FTO counter

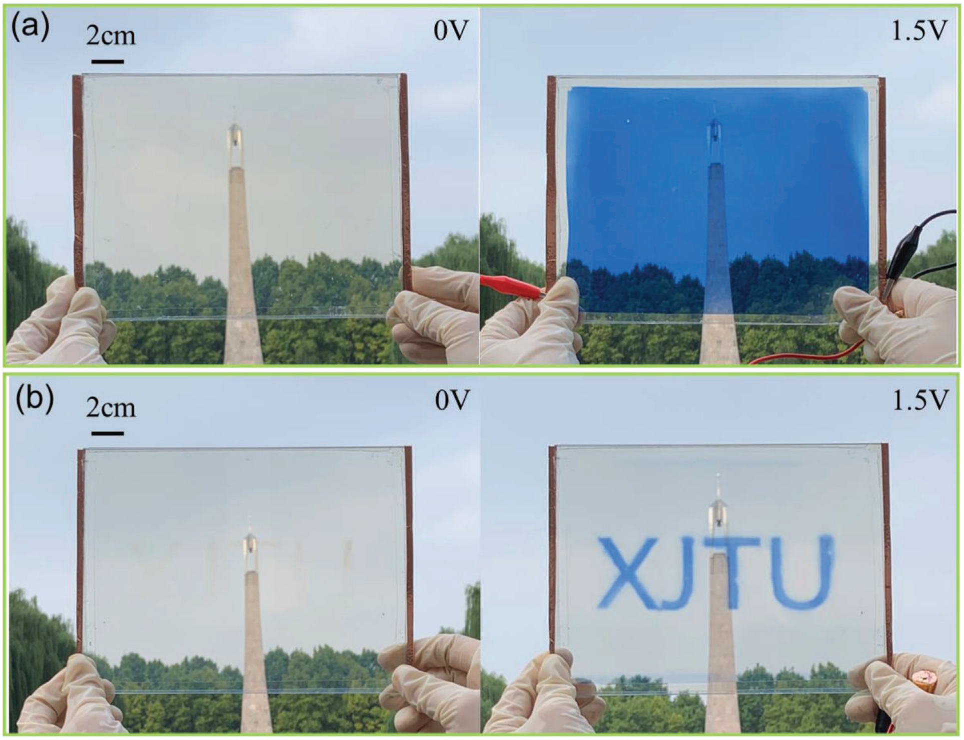

**Figure 5.** a) Photographs of the bleached and colored large area smart windows. b) Photographs of the transparent electrochromic display device.

electrodes. As shown in **Figure 5**a, by spraying the $CuO_x$ precursor on FTO glass, we assembled a smart window with the size of 15 cm × 20 cm. The conductive copper tape is attached to the edge of the electrodes for better voltage application. Surprisingly, such a large area of smart window can be powered by a single dry battery, with an open circuit voltage of only 1.5 V. As a comparison, a large area electrochromic device with bare FTO counter electrode was also operated using the same battery in Figure S9 (Supporting information). The relatively uniform coloring process shown in Figure 5a strongly proves that the $CuO_x$/FTO counter electrodes can reduce power consumption in practical electrochromic devices. In addition to smart windows, the apparent color difference between the two states of the electrochromic device can be used for information display.[59–61] As previously mentioned, the reduction reaction of viologen corresponding to coloring process on the working electrode is synchronized with the oxidation reaction of $Br^-$ ions on the counter electrode. The reduction reaction of viologen cations will preferentially proceed on the working electrode corresponding $CuO_x$ modified FTO counter electrode, which can enable local coloring and be used for information display. Based on this principle, an electrochromic display device is designed using the $CuO_x$ partially modified FTO counter electrode. The electrochromic device with "XJTU" patterned counter electrode is shown in Figure 5b. The high transparency and barely visible "XJTU" patterns in this electrochromic device are due to the high transmittance of $CuO_x$/FTO electrode. And the device can display the obvious blue "XJTU" letters when the device is driven by a single dry battery (1.5 V). This low driving voltage transparent electrochromic display provides a new scenario for the application of $CuO_x$/FTO counter electrode, which has great potential in energy-saving human-machine interface.

## 3. Conclusion

In summary, we have successfully demonstrated a high performance viologen based electrochromic device with $CuO_x$ modified FTO counter electrode. The $CuO_x$ nanoparticles were deposited on the surface of FTO electrode by a low cost sol-gel method, which provides catalytic sites without sacrificing the transparency of the device. It is found that $CuO_x$ exhibits excellent electrocatalytic activity for $Br^-/Br_3^-$ redox couple, leading to a dramatically improved electrochemical reaction during the coloring process. The resulted electrochromic device shows a much better cycling stability performance compared to the control sample with bare FTO counter electrode, and the driving voltage reduced from 1.8 to 1.3 V. Furthermore, large area electrochromic devices (15 cm × 20 cm) with $CuO_x$/FTO counter electrode have been prepared by spraying, which can be powered by a 1.5 V dry battery. This work provides a facile strategy to improve the electrochromic devices via counter electrode interface functionalization and sheds light on the optoelectronic application of catalysis.

## 4. Experimental Section

*Materials*: Copper chloride anhydrous ($CuCl_2$, 99%) was purchased from Sinopharm chemical reagent Co., Ltd. Citric acid (99.5%) was purchased from Tianjin Kemiou chemical reagent Co., Ltd. Ethyl viologen dibromide (98%) and propylene carbonate (99.7%) were purchased from

Shanghai Aladdin bio-chem technology Co., Ltd. Fluorine-doped tin oxide (FTO) glasses were purchased from Liaoning Youxuan New Energy Technology Co., Ltd.

*Fabrication of $CuO_x$ Electrocatalytic Electrode*: The $CuO_x$ modified FTO conductive glass was used as the electrocatalytic counter electrode in this work. It was synthetized by a simple and low-cost sol–gel method. To achieve $CuO_x$ precursor, 0.1 g $CuCl_2$ and 0.05 g citric acid were added into 10 g DI water at room temperature. Then, the mixture was stirred for 30 min and aged overnight. Afterward, the precursor was spin-coated or spray-coated on the FTO glasses at 4000 r $min^{-1}$ for 10 s. The samples were dried and annealed on a hot plate at 380 °C for 30 min. In addition, the sample for XRD testing was prepared by drop coating method using the same CuOx precursor. Besides, the patterned CuOx film was prepared through a mask during the spraying process.

*Preparation of the Electrochromic Device with $CuO_x$/FTO Counter Electrode*: The ethyl viologen dibromide was dissolved in propylene carbonate with a concentration of 5 mg $ml^{-1}$ to get the electrolyte. Meanwhile, the working electrode (bare FTO glass) and the electrocatalytic counter electrode (CuOx modified FTO glass) were packaged face to face, with 1 mm pitch. Then, the ethyl viologen electrolyte was filled in the space and then sealed by silicon rubber. The control samples were fabricated by the same assembly process, but both the working electrode and counter electrode are bare FTO glasses.

*Characterization*: The chemical valence of $CuO_x$ is identified by X-ray photoelectron spectroscopy and Auger spectra (XPS, Thermo Scientific K-Alpha, Thermo Fisher Scientific, USA). The crystallography of the $CuO_x$ was confirmed by X-ray diffraction (D8 ADVANCE, BRUKER, Germany), high-resolution transmission electron microscopy (FEI Tecnai 20, US) and Raman spectrometer (InVia Qontor, Renishaw, Britain). The morphology of the $CuO_x$ modified FTO glass was observed by field emission scanning electron microscopy (GeminiSEM 500, Zeiss, Germany). The transmittance measurements of the electrodes and electrochromic devices were carried out by a spectrometer (V-1600 PC, Shanghai Mepeda Instrument Co., Ltd, China). The current of the device was measured by a digital sourcemeter (Keithley 2410, USA). The cyclic voltammogram curve was tested by an electrochemical workstation (Zennium Pro, Zahner, Germany).

## Supporting Information

Supporting Information is available from the Wiley Online Library or from the author.

## Acknowledgements

This work was supported by the National Natural Science Foundation of China (No. 51902250). H.J.F. thanks the support from the Guangdong Provincial Key Laboratory Program (Grant No. 2021B1212040001). H.W. acknowledged the support of the Shenzhen Science and Technology Innovation Program (No. KQTD20180411143514543). L.L.W. thanks the support of the Fundamental Research Program of Shanxi Province (No. 202203021222023). Instrument Analysis Center of Xi'an Jiaotong University is acknowledged for the great help in measurements.

## Conflict of Interest

The authors declare no conflict of interest.

## Data Availability Statement

The data that support the findings of this study are available from the corresponding author upon reasonable request.

## Keywords

Copper oxides, counter electrodes, electrocatalysis, energy saving, viologen-based electrochromic devices

Received: June 22, 2023
Revised: August 31, 2023

---

[1] W. Wu, H. Fang, H. Ma, L. Wu, W. Zhang, H. Wang, *Nano-Micro Lett.* **2021**, *13*, 20.
[2] D. Ma, A. Lee-Sie Eh, S. Cao, P. S. Lee, J. Wang, *ACS Appl. Mater. Interfaces* **2022**, *14*, 1443.
[3] Z. Sun, X. Xie, W. Xu, K. Chen, Y. Liu, X. Chu, Y. Niu, S. Zhang, C. Ren, *ACS Sustainable Chem. Eng.* **2021**, *9*, 12949.
[4] Y. Shi, G. Wang, Q. Chen, J. Zheng, C. Xu, *Sol. Energy Mater Sol. Cells* **2020**, *208*, 110413.
[5] H. Fang, P. Zheng, R. Ma, C. Xu, G. Yang, Q. Wang, H. Wang, *Mater. Horiz.* **2018**, *5*, 1000.
[6] A. L. Dyer, R. H. Bulloch, Y. Zhou, B. Kippelen, J. R. Reynolds, F. Zhang, *Adv. Mater.* **2014**, *28*, 4895.
[7] C. Wu, Z. Shao, W. Zhai, X. Zhang, C. Zhang, C. Zhu, Y. Yu, W. Liu, *ACS Nano* **2022**, *16*, 2621.
[8] H. Gu, C. Guo, S. Zhang, L. Bi, T. Li, T. Sun, S. Liu, *ACS Nano* **2018**, *12*, 559.
[9] K.-W. Kim, J. K. Lee, X. Tang, Y. Lee, J. Yeo, H. C. Moon, S. W. Lee, S. H. Kim, *Dyes Pigm.* **2021**, *190*, 109321.
[10] X.-C. Lin, N. Li, W.-J. Zhang, Z.-J. Huang, Q. Tang, C. Gong, X.-K. Fu, *Dyes Pigm.* **2019**, *171*, 107783.
[11] S.-Y. Kao, Y. Kawahara, S. i. Nakatsuji, K.-C. Ho, *J. Mater. Chem. C* **2015**, *3*, 3266.
[12] H.-C. Lu, S.-Y. Kao, H.-F. Yu, T.-H. Chang, C.-W. Kung, K.-C. Ho, *ACS Appl. Mater. Interfaces* **2016**, *8*, 30351.
[13] H. Huang, H. Li, X. Shen, K. Gu, J. Guo, C. Wang, *Chem. Eng. J.* **2022**, *429*, 132437.
[14] J.-W. Kim, J.-M. Myoung, *Adv. Funct. Mater.* **2019**, *29*, 1808911.
[15] G. Li, B. Zhang, J. Wang, H. Zhao, W. Ma, L. Xu, W. Zhang, K. Zhou, Y. Du, G. He, *Angew. Chem., Int. Ed. Engl.* **2019**, *58*, 8468.
[16] L.-Y. Hsiao, F.-Y. Kuo, C.-H. Wu, Y.-C. Huang, Y.-C. Wang, R.-J. Jeng, K.-C. Ho, *Chem. Eng. J.* **2021**, *420*, 129821.
[17] P. Zhang, X. Xing, Y. Wang, I. Murtaza, Y. He, J. Cameron, S. Ahmed, P. J. Skabara, H. Meng, *J. Mater. Chem. C* **2019**, *7*, 9467.
[18] N. Kobayashi, S. Miura, M. Nishimura, H. Urano, *Sol. Energy Mater. Sol. Cells* **2008**, *92*, 136.
[19] L. Wu, H. Fang, C. Zheng, Q. Wang, H. Wang, *J. Mater. Chem. C* **2019**, *7*, 10446.
[20] J. M. C. Puguan, H. Kim, *J. Mater. Chem. A* **2019**, *7*, 21668.
[21] Z. Wang, K. Shen, H. Xie, B. Xue, J. Zheng, C. Xu, *Chem. Eng. J.* **2021**, *426*, 121214.
[22] L.-C. Chen, Y.-H. Huang, K.-C. Ho, *J. Solid State Electrochem.* **2002**, *7*, 6.
[23] S. Tsuneyasu, Y. Watanabe, K. Nakamura, N. Kobayashi, *Sol. Energy Mater. Sol. Cells* **2017**, *163*, 200.
[24] S. Bogati, R. Basnet, A. Georg, *Sol. Energy Mater. Sol. Cells* **2019**, *189*, 206.
[25] F. Xi, H. Liu, W. Li, L. Zhu, H. Geng, L. Quan, W. Liang, *Electrochim. Acta* **2015**, *178*, 329.
[26] M. Chen, R.-H. Zha, Z.-Y. Yuan, Q.-S. Jing, Z.-Y. Huang, X.-K. Yang, S.-M. Yang, X.-H. Zhao, D.-L. Xu, G.-D. Zou, *Chem. Eng. J.* **2017**, *313*, 791.
[27] C. Liu, M. Hirohara, T. Maekawa, R. Chang, T. Hayashi, C.-Y. Chiang, *Appl. Catal. B* **2020**, *265*, 118543.

[28] K. A. Adegoke, N. W. Maxakato, *Mater. Today Energy* **2021**, *21*, 100816.

[29] X. Du, M. A. Oturan, M. Zhou, N. Belkessa, P. Su, J. Cai, C. Trellu, E. Mousset, *Appl. Catal. B* **2021**, *296*, 120332.

[30] W.-Y. Huo, S.-Q. Wang, W.-H. Zhu, Z.-L. Zhang, F. Fang, Z.-H. Xie, J.-Q. Jiang, *Tungsten* **2021**, *3*, 161.

[31] Y. Meng, Y. Chen, J. Zhu, Y. Qi, J. Ding, W. Zhou, *Mater. Horiz.* **2021**, *8*, 972.

[32] Z. Pan, E. Han, J. Zheng, J. Lu, X. Wang, Y. Yin, G. I. N. Waterhouse, X. Wang, P. Li, *Nano-Micro Lett.* **2020**, *12*, 18.

[33] R. Chen, Z. Ren, Y. Liang, G. Zhang, T. Dittrich, R. Liu, Y. Liu, Y. Zhao, S. Pang, H. An, C. Ni, P. Zhou, K. Han, F. Fan, C. Li, *Nature* **2022**, *610*, 296.

[34] D. Jiang, J. Xue, L. Wu, W. Zhou, Y. Zhang, X. Li, *Appl. Catal. B* **2017**, *211*, 199.

[35] C. V. V. Muralee Gopi, R. Vinodh, S. Sambasivam, I. M. Obaidat, R. M. Naidu Kalla, H.-J. Kim, *Mater. Today Energy* **2019**, *14*, 100358.

[36] S. Sukumar, A. Rudrasenan, D. Padmanabhan Nambiar, *ACS Omega* **2020**, *5*, 1040.

[37] S. Velu, K. Suzuki, C. S. Gopinath, H. Yoshida, T. Hattori, *Phys. Chem. Chem. Phys.* **2002**, *4*, 1990.

[38] Y. Xie, M. Gao, H. Zhang, S. Zeng, X. Zhao, Y. Zhao, H. Su, J. Song, X. Li, Q. Jia, *Int. J. Hydrogen Energy* **2016**, *47*, 21979.

[39] J. P. Espinós, J. Morales, A. Barranco, A. Caballero, J. P. Holgado, A. R. González-Elipe, *J. Phys. Chem. B* **2002**, *106*, 6921.

[40] T. S. Cam, S. O. Omarov, M. I. Chebanenko, A. S. Sklyarova, V. N. Nevedomskiy, V. I. Popkov, *J. Environ. Chem. Eng.* **2021**, *9*, 105373.

[41] H. Siddiqui, M. S. Qureshi, F. Z. Haque, *Nano-Micro Lett.* **2020**, *12*, 29.

[42] Y. Xu, Y. Wen, T. Ren, H. Yu, K. Deng, Z. Wang, X. Li, L. Wang, H. Wang, *Appl. Catal. B* **2023**, *320*, 121981.

[43] M. A. Bajiri, A. Hezam, K. Namratha, R. Viswanath, Q. A. Drmosh, H. S. Bhojya Naik, K. Byrappa, *J. Environ. Chem. Eng.* **2019**, *7*, 103412.

[44] A. Umar, H. Algadi, R. Kumar, M. S. Akhtar, A. A. Ibrahim, H. Albargi, M. A. M. Alhamami, T. Alsuwian, W. Zeng, *Chemosensors* **2021**, *9*, 221.

[45] W. Niu, J. Shi, L. Ju, Z. Li, N. Orlovskaya, Y. Liu, Y. Yang, *ACS Catal.* **2018**, *8*, 12030.

[46] T. H. Tran, M. H. Nguyen, T. H. T. Nguyen, V. P. T. Dao, Q. H. Nguyen, C. D. Sai, N. H. Pham, T. C. Bach, A. B. Ngac, T. T. Nguyen, K. H. Ho, H. Cheong, V. T. Nguyen, *Appl. Surf. Sci.* **2020**, *509*, 145325.

[47] D. Butmanov, T. Savchuk, I. Gavrilin, D. Dronova, A. Savitskiy, I. Tsiniaikin, A. Dronov, S. Gavrilov, *Phys. E* **2023**, *146*,115533.

[48] H. Fang, L. Wu, H. Ma, W. Wu, L. Wu, Y. Zhang, H. Wang, *Chem. Eng. J.* **2022**, *438*, 135383.

[49] P. Yang, P. Sun, Z. Chai, L. Huang, X. Cai, S. Tan, J. Song, W. Mai, *Angew. Chem., Int. Ed. Engl.* **2014**, *53*, 11935.

[50] K. Madasamy, D. Velayutham, V. Suryanarayanan, M. Kathiresan, K.-C. Ho, *J. Mater. Chem. C* **2019**, *7*, 4622.

[51] B. Gelinas, D. Das, D. Rochefort, *ACS Appl. Mater. Interfaces* **2017**, *9*, 28726.

[52] X. Wang, L. Guo, S. Cao, W. Zhao, *Chem. Phys. Lett.* **2020**, *749*, 137434.

[53] J.-W. Kim, J.-M. Myoung, *Adv. Funct. Mater.* **2019**, *29*, 1808911.

[54] H. Ling, J. Wu, F. Su, Y. Tian, Y. J. Liu, *Nat. Commun.* **2021**, *12*, 1010.

[55] F. Xi, H. Liu, W. Li, L. Zhu, H. Geng, L. Quan, W. Liang, *Electrochim. Acta* **2015**, *178*, 329.

[56] L. Li, H. Yang, J. Miao, L. Zhang, H.-Y. Wang, Z. Zeng, W. Huang, X. Dong, B. Liu, *ACS Energy Lett.* **2017**, *2*, 294.

[57] W. Xu, G. Fan, J. Chen, J. Li, L. Zhang, S. Zhu, X. Su, F. Cheng, J. Chen, *Angew. Chem., Int. Ed. Engl.* **2020**, *59*, 3511.

[58] J. Zheng, Y. Lyu, M. Qiao, R. Wang, Y. Zhou, H. Li, C. Chen, Y. Li, H. Zhou, S. P. Jiang, S. Wang, *Chem* **2019**, *5*, 617.

[59] H. Fang, Z. Zhao, W. Wu, H. Wang, *J. Inorg. Mater.* **2021**, *36*, 140.

[60] S. Bi, W. Jin, X. Han, X. Cao, Z. He, K. Asare-Yeboah, C. Jiang, *Nano Energy* **2022**, *102*, 107629.

[61] K. Chen, Y. Wu, L. You, W. Wu, X. Wang, D. Zhang, J. F. Elman, M. Ahmed, H. Wang, K. Zhao, J. Mei, *Mater. Horiz.* **2022**, *9*, 425.